Supporting information for

Buffering the local pH via single-atomic Mn-N auxiliary sites to boost CO_2 electroreduction

Yan Yang, [abe] Tang Tang,[a] Zhen-Hua Lyu,[ae] Li-Rong Zheng,[c] Qing-Hua Zhang, [d] Jiaju Fu,*[a] and Jin-Song Hu*[aef]

a. Beijing National Laboratory for Molecular Sciences (BNLMS), CAS Key Laboratory of Molecular Nanostructure and Nanotechnology, Institute of Chemistry, Chinese Academy of Sciences, Beijing 100190, China. E-mail: fujiaju@iccas.ac.cn; hujs@iccas.ac.cn

b. Zhejiang Tiandi Environmental Protection Technology Co., Ltd, Hangzhou 310003, China.

c. Institute of High Energy Physics, Chinese Academy of Sciences, Beijing 100049, China.

d. Institute of Physics, Chinese Academy of Sciences, Beijing 100190, China.

e. University of Chinese Academy of Sciences, Beijing 100049, China.

f. Dalian National Laboratory for Clean Energy, Dalian 116023, China.

Table of Contents

Table S1. Elemental contents calculated from ICP-AES results.

Table S2. Comparison of other Ni SACs for the electrochemical conversion of CO_2 to CO.

Experimental procedures

I. Synthesis

***Materials*:** Potassium citrate monohydrate ($K_3C_6H_5O_7 \cdot H_2O$, 99+%, Alfa Aesar Co., Ltd.), nickel nitrate hexahydrate ($Ni(NO_3)_2 \cdot 6H_2O$, 99%, Alfa Aesar Co., Ltd.), manganese nitrate hexahydrate ($Mn(NO_3)_2 \cdot 6H_2O$, 99%, Alfa Aesar Co., Ltd.), α-D-glucose ($C_6H_{12}O_6$, 99%, Alfa Aesar Co., Ltd.), melamine ($C_3H_6N_6$, 99%, Alfa Aesar Co., Ltd.), potassium bicarbonate ($KHCO_3$, 99.7-100.5%, Alfa Aesar Co., Ltd.), sulfuric acid (H_2SO_4, 95-98%, Sinopharm Chemical Reagent Co. Ltd).

***Preparation of porous carbon (PC)*:** 2.5 g $K_3C_6H_5O_7 \cdot H_2O$ was pyrolyzed at 800°C for one hour under Ar atmosphere to obtain a black product (heating rate 3°C /min), followed by post-processing with 0.5 M H_2SO_4 solution and deionized water to remove inorganic impurities until the pH was close to 7. Then obtained power went through a wet ball milling at 500 rpm for 4 h with isopropanol as solvent. The precipitates were collected by centrifugation and drying at 60°C.

***Preparation of Ni/Mn-N-C*:** Typically, 0.75 mmol of $Ni(NO_3)_2 \cdot 6H_2O$ and 0.75 mmol of $Mn(NO_3)_2 \cdot 6H_2O$ were first dissolved in 5 mL of deionized water. Then, 1.2 g of α-D-glucose and 60 mg of ball-milled porous carbon were added to the above solution and sonicated for 30min, followed by a 12 h store. The precipitates were then separated by centrifugation at 6000 rpm for 3 min, drying at 60°C overnight, and then grounded by melamine with a mass radio of 1:5. The obtained power went through pyrolysis at 800 °C for two hours under the Ar atmosphere.

***Preparation of Ni-N-C*:** Typically, 1.50 mmol of $Ni(NO_3)_2 \cdot 6H_2O$ was first dissolved in 5 mL of deionized water. Then, 1.2 g of α-D-glucose and 60 mg of ball-milled porous carbon were added to the above solution and sonicated for 30min, followed by a 12 h store. The precipitates were then separated by centrifugation at 6000 rpm for 3 min, drying at 60°C overnight, and then grounded by melamine with a mass radio of 1:5. The obtained power went through pyrolysis at 800 °C for two hours under the Ar atmosphere.

***Preparation of Mn-N-C*:** Typically, 1.50 mmol of $Mn(NO_3)_2 \cdot 6H_2O$ was first dissolved in 5 mL of deionized water. Then, 1.2 g of α-D-glucose and 60 mg of ball-milled porous carbon were added to the above solution and sonicated for 30min, followed by a 12 h store. The precipitates were then separated by centrifugation at 6000 rpm for 3 min, drying at 60°C overnight, and then grounded by melamine with a mass radio of 1:5. The obtained power went through pyrolysis at 800 °C for two

hours under the Ar atmosphere.

II. Characterizations

The Powder X-ray diffraction (XRD) pattern was performed on a Rigaku D/Max-2500 diffractometer using a Cu Kα1 radiation (λ = 1.54 Å). Scanning electron microscopic images (SEM) were obtained on a Hitachi scanning electron microscope (S-4800, Japan). Transmission electron microscopic (TEM) images were collected by the JEM-2100F microscope (JEOL, Tokyo, Japan) equipped with an EDS detector (Oxford Instrument, UK), working at an acceleration voltage of 200 kV. STEM images were attained on a JEOL ARM200F (JEOL, Tokyo, Japan) STEM under 200 kV with a cold filed-emission gun and double hexapole Cs correctors (CEOS GmbH, Heidelberg, Germany). Electron energy loss spectroscopy (EELS) data were obtained with a multi-scan charge-coupled device (CCD) camera (Gatan Quantum Model 965, Gatan Inc.). X-ray photoelectron spectroscopy (XPS) analysis was performed on an ESCALab220i-XL electron spectrometer (VG Scientific, UK) using a monochromatic Al Kα radiation as the X-ray source. T X-ray absorption spectroscopy (XAS) of Cu K-edge was obtained on the XAFS station of the 3W1 beamline of the Beijing Synchrotron Radiation Facility (BSRF) using a Si (111) double crystal monochromator.

III. Electrochemical measurements

Electrochemical CO_2RR measurements were performed at ambient pressure and room temperature using a standard three-electrode system configured with an H-type electrolytic cell, in which an electrode prepared from a catalyst, an Ag/AgCl electrode, and a graphite rod were used as the working electrode, reference electrode, and counter electrode, respectively. 15 mL of 0.5 M $KHCO_3$ solution (pH=7.2) was added to the anode compartment and the cathode compartment, respectively, and the gas space was 10 mL, which was separated by a Nafion-117 proton exchange membrane. Before measurement, the cathode compartment was pre-saturated by purging with high purity CO_2/Ar for at least 30 min. During the measurement, the flow rate of CO_2 blown into the electrolyte was fixed at 10 mL min^{-1}. Linear sweep voltammetry was performed in CO_2/Ar-saturated 0.5 M $KHCO_3$ aqueous solution with a potential range of 0.20 V to -1.20 V and a scan rate of 5 mV s^{-1}. The C_{dl} values were determined from the cyclic voltammograms (CVs) of the electric double layer region at different scan rates. The potential sweep range of the CV curve was from 0.20 V to 0.40 V, and the sweep speed ranged from 10 mV s^{-1} to 60 mV s^{-1}.

All potentials mentioned in this work were converted to the values vs. reversible hydrogen electrode (RHE) followed by the Nernst equation (1):

E (*vs* RHE) = E (*vs* Ag/AgCl) +0.198+0.059 × pH.

The Faradaic efficiency (FE) of the specific products was calculated by the following equation (2):

$FE_i = Q_i/Q_{total} = z \times n_i \times F/Q_{total}$

i: the specific products including CO, H_2;

Q_i: the partial charge used for the generation of specific products, C;

Q_{total}: the total charge passed, C;

z: the number of transferred electrons for CO_2-to-CO conversion and H_2O-H_2 reduction, which is two for CO and H_2;

n_i: the number of moles for specific products;

F: Faradaic constant, which is 96,485 C mol^{-1};

All current densities (mA cm^{-2}) mentioned in this article were normalized to the electrode geometrical area.

Gas chromatography (GC, Agilent Technologies 7890B) was employed to detect gaseous products generated from the cathode compartment. ^{1}H Nuclear magnetic resonance (NMR, Bruker AVANCE 600) was employed to analyze the liquid products containing the mixture of 500 μL electrolyte after electrocatalysis, 100 μL of D_2O, and 100 μL of 7.0 mM of dimethyl sulphoxide solution (DMSO, internal standard).

IV. The preparation of working electrodes

Typically, the mixed solution contains 2 mg of catalyst powder, 760 μL of ethanol, and 40 μL of 0.5 wt.% Nafion solution was sonicated for 30 min to form a uniform catalyst ink. The catalyst ink (400μL) was then uniformly dropped onto the carbon paper (CP), giving a catalyst loading of 1.0 mg cm^{-2}. The working electrode was naturally dried for the following electrochemical test.

V. Local pH Characterization

The catalyst ink solution containing 2 mg of catalyst powder and 500 μL of ethanol was sonicated for 30 min to form a uniform catalyst ink. The catalyst ink (12 μL) and 0.5 wt.% Nafion solution (5

μL) were then uniformly dropped onto the surface of disk electrodes successively. The disk electrode was naturally dried for the following electrochemical test.

The electrochemical test was performed in a standard three-electrode cell using a rotating ring disk electrode assembly equipped with a bipotentiostat (CHI 760E). Ag/AgCl electrodes and graphite rods were used as reference and counter electrodes, respectively. 25 mL of 0.5 M $KHCO_3$ solution was added to the electrolytic cell, and it was pre-saturated by purging with high-purity CO_2 for at least 30 minutes before measurement. During the test, CO_2 gas was continuously passed into the electrolyte to ensure that the pH was stable at 7.2. The rotating ring disk electrode (RRDE) assembly consisted of the as-prepared catalyst disks (Ni/Mn-N-C, Ni-N-C, and Mn-N-C) and Pt ring electrodes. Under rotating conditions (1600 rpm), a specific negative potential (ranging from -0.56 V to -0.96 V) was applied to the catalyst disc to catalyze CO_2RR to CO, while the Pt ring electrode was subjected to a CV cycle between 0 and 1.2 V at a scan rate of 100 mV^{-1}.

Supporting Figures

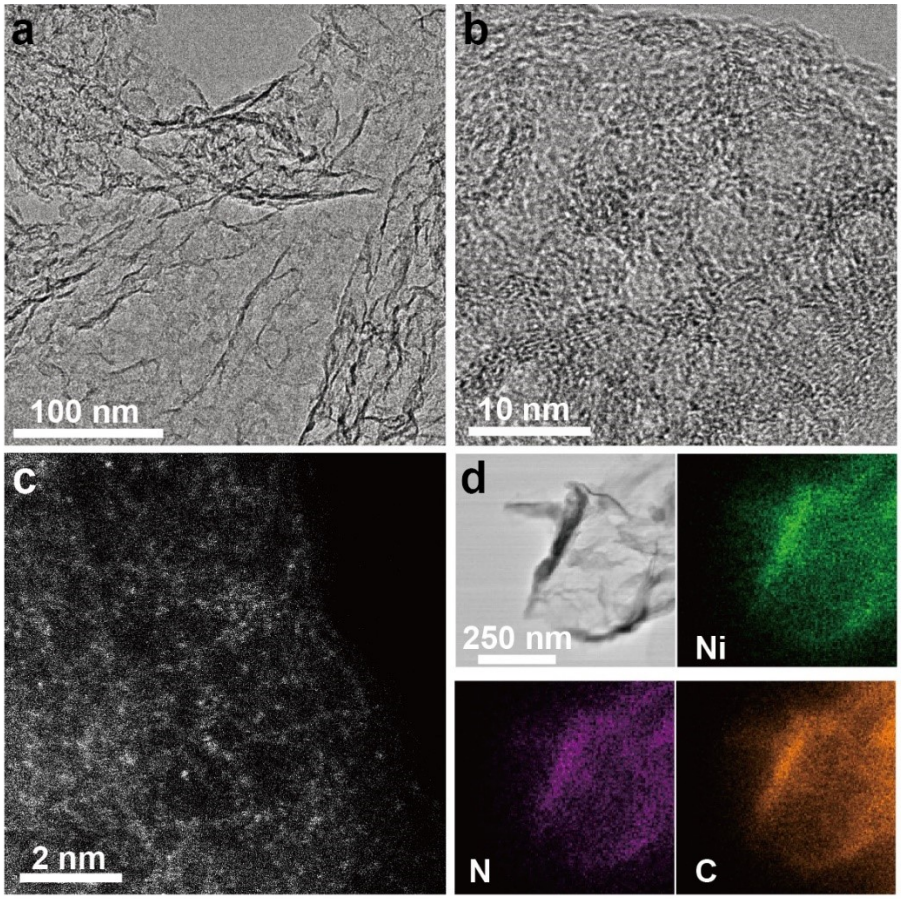

Figure S1. a) TEM image of Ni-N-C, b) HRTEM image of Ni-N-C, c) HAADF-STEM image of Ni-N-C, d) TEM image and corresponding elemental mapping images of Ni-N-C.

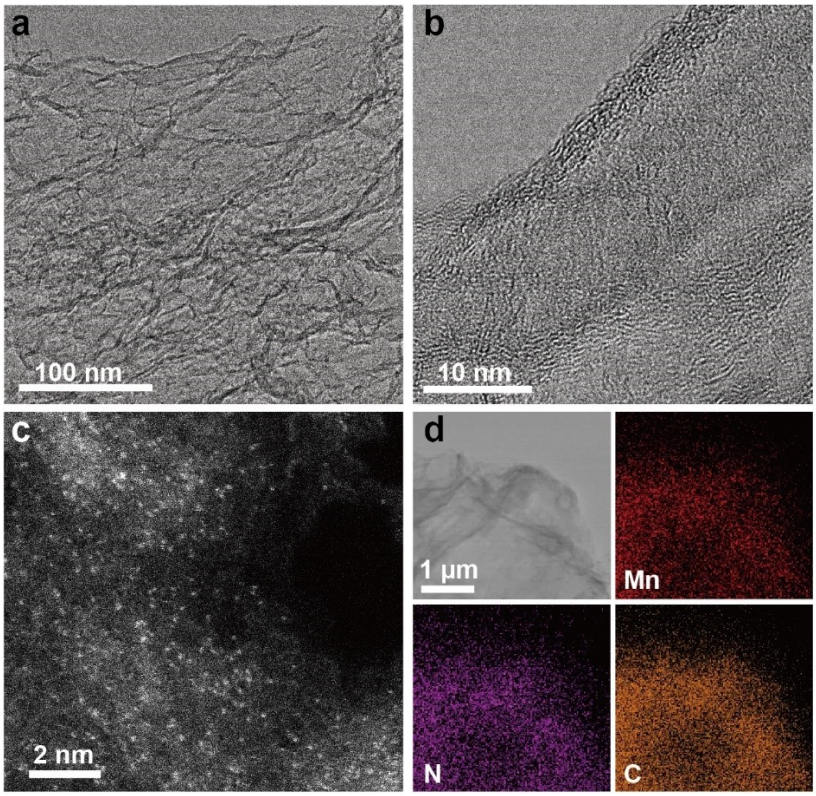

Figure S2. a) TEM image of Mn-N-C, b) HRTEM image of Mn-N-C, c) HAADF-STEM image of Mn-N-C, d) TEM image and corresponding elemental mapping images of Mn-N-C.

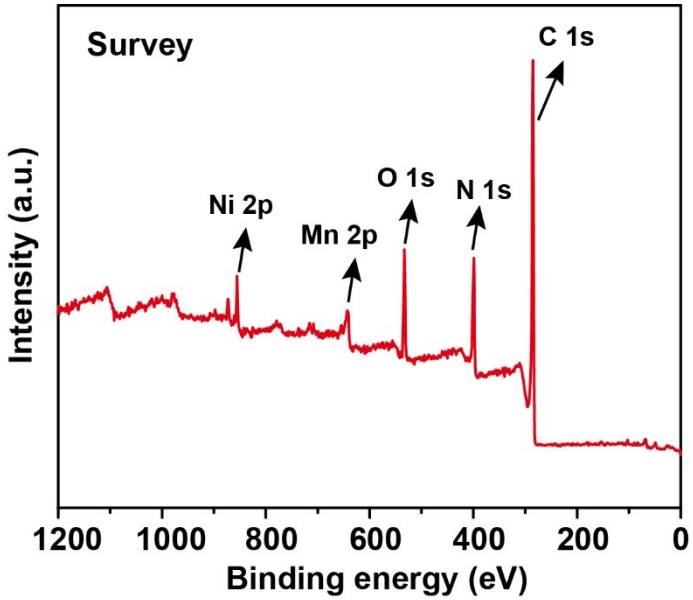

Figure S3. The survey XPS spectra of Ni/Mn-N-C.

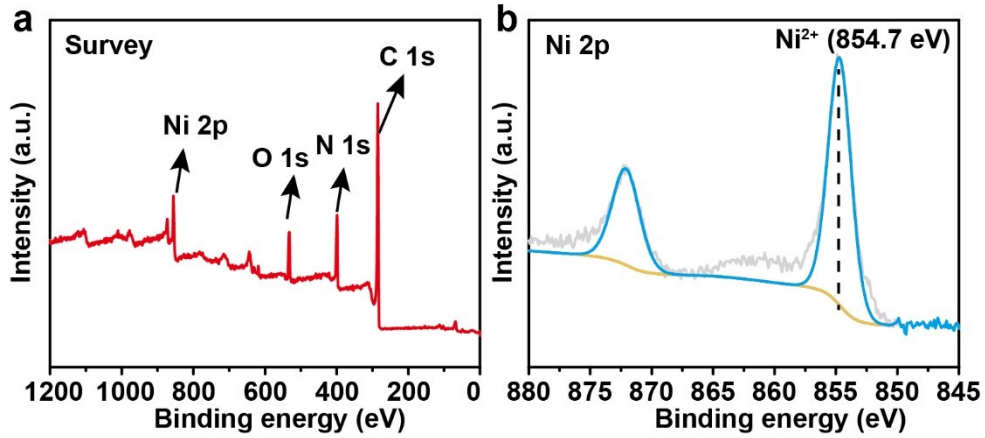

Figure S4. a) The survey XPS spectra of Ni-N-C, b) The Ni 2p XPS spectra of Ni-N-C.

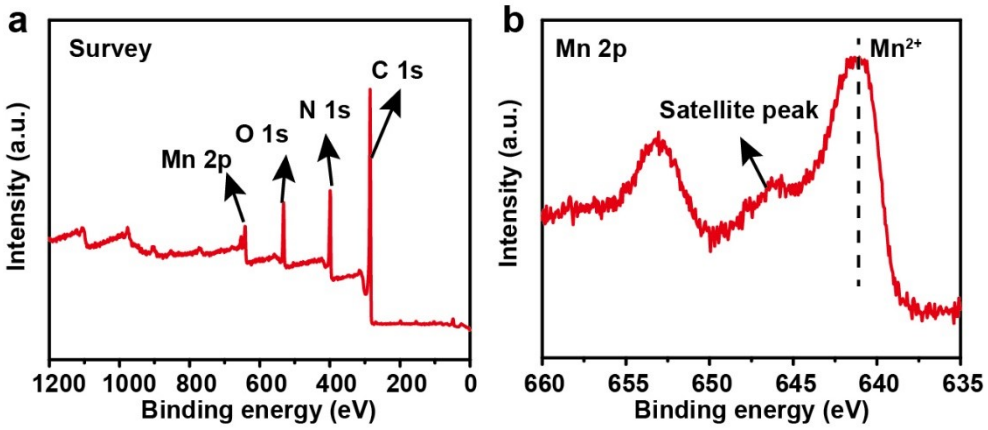

Figure S5. a) The survey XPS spectra of Mn-N-C, b) The Mn 2p XPS spectra of Mn-N-C.

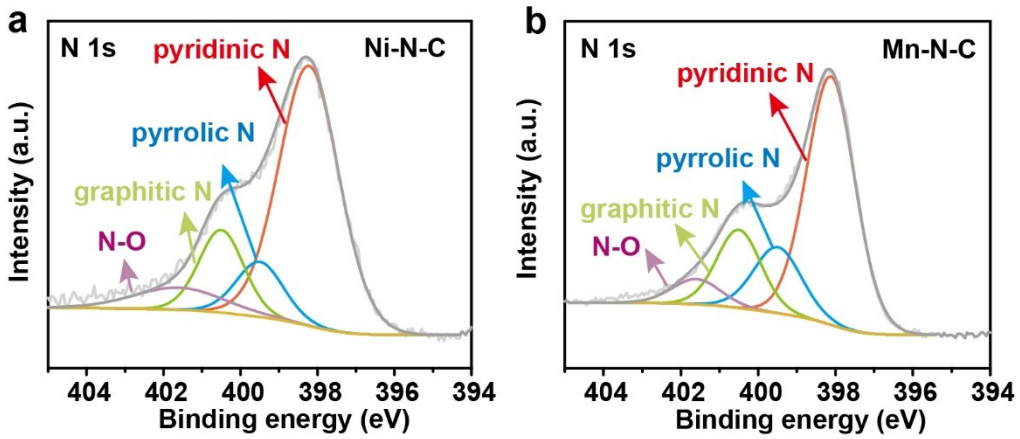

Figure S6. a) The high-resolution N 1s XPS spectra of Ni-N-C, b) The high-resolution N 1s XPS spectra of Mn-N-C.

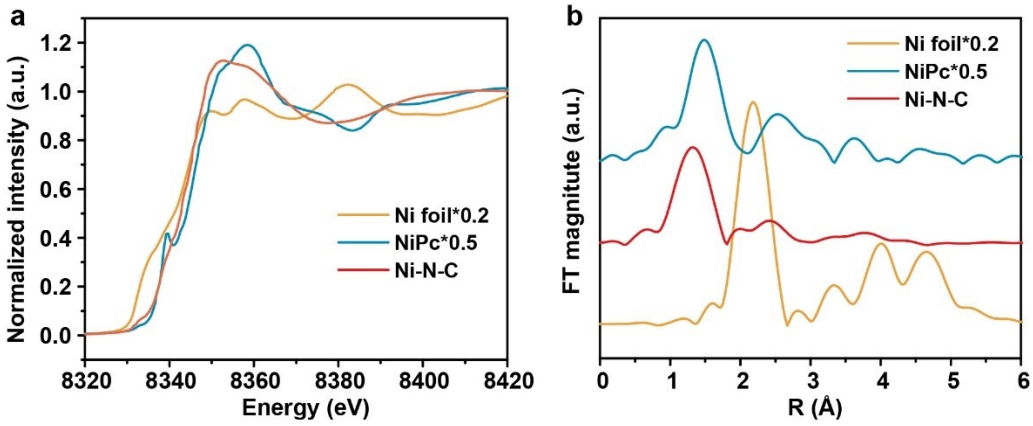

Figure S7. a) Ni K edge XANES spectra of Ni-N-C, b) Ni K edge EXAFS spectra of Ni-N-C.

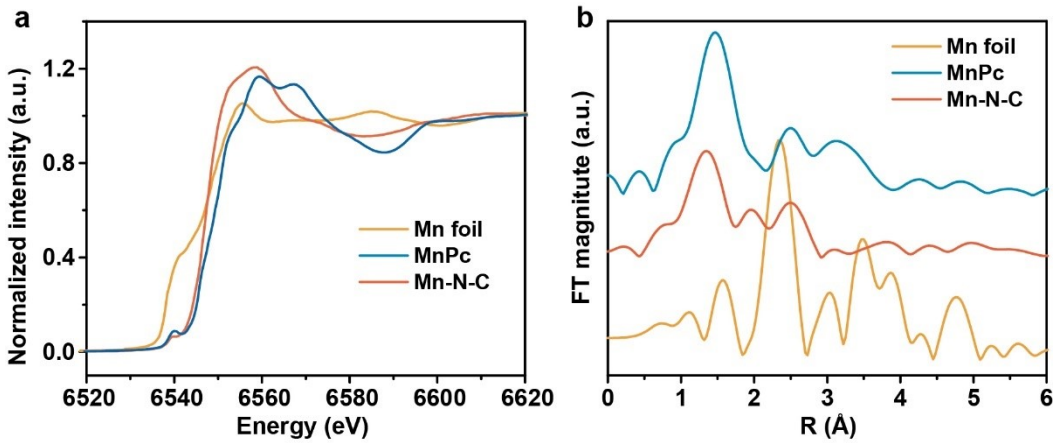

Figure S8. a) Mn K edge XANES spectra of Mn-N-C, b) Mn K edge EXAFS spectra of Mn-N-C.

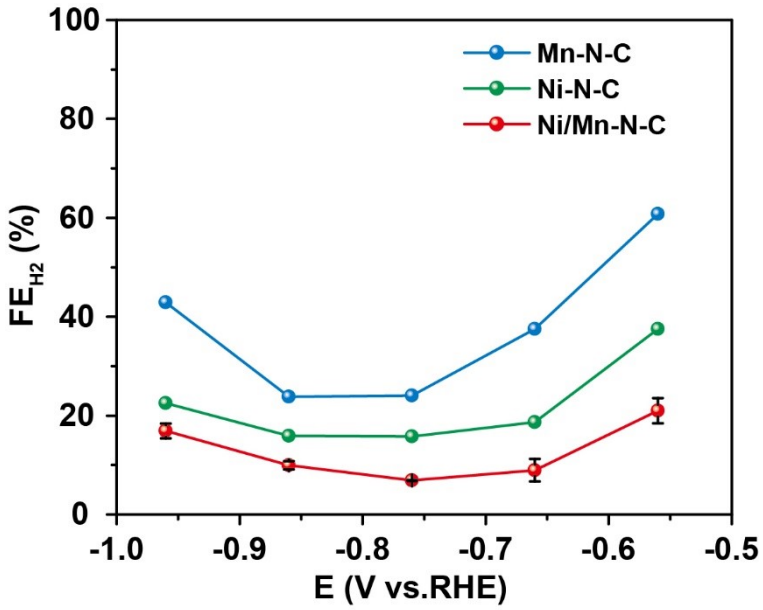

Figure S9. Potential-dependent FEs for H_2 of Ni/Mn-N-C, Ni-N-C, and Mn-N-C.

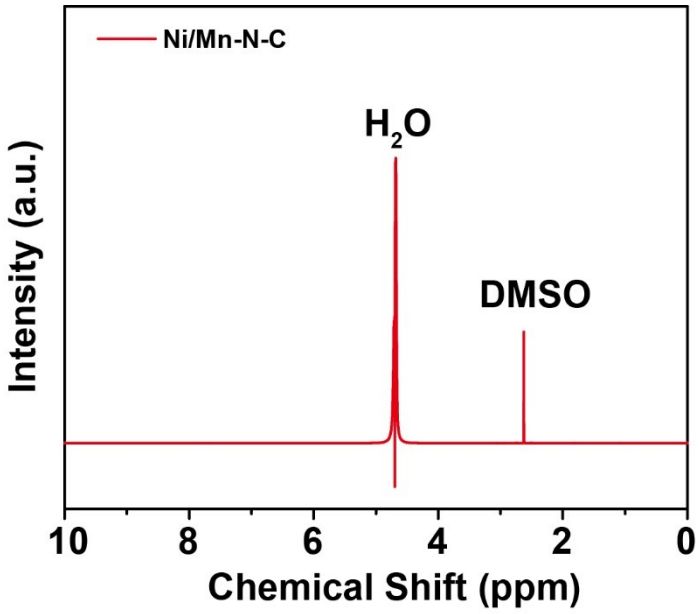

Figure S10. Characterization for the liquid product of Ni/Mn-N-C after 3 h CO_2 reduction at -0.76V process by nuclear magnetic resonance spectroscopy.

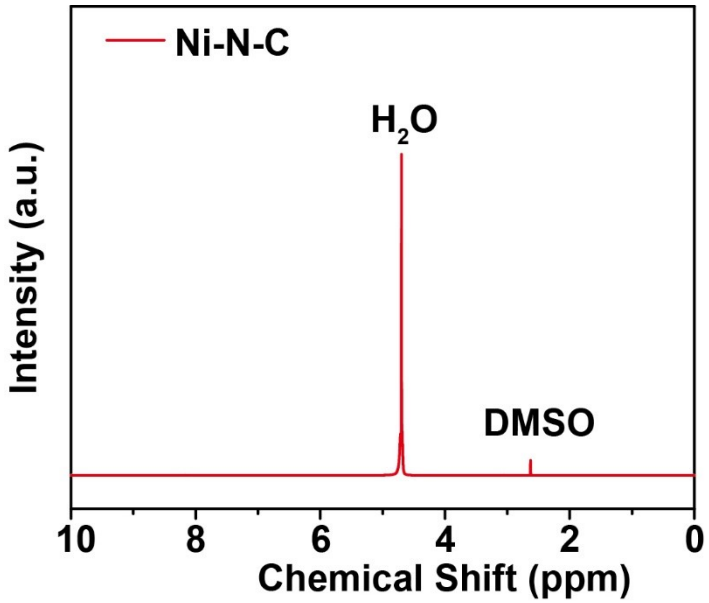

Figure S11. Characterization for the liquid product of Ni-N-C after 3 h CO_2 reduction at -0.76V process by nuclear magnetic resonance spectroscopy.

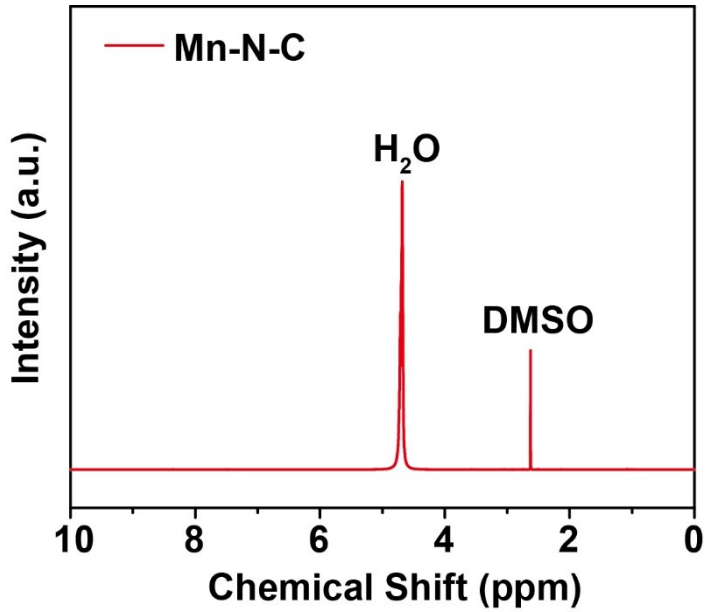

Figure S12. Characterization for the liquid product of Mn-N-C after 3 h CO_2 reduction at -0.76V process by nuclear magnetic resonance spectroscopy.

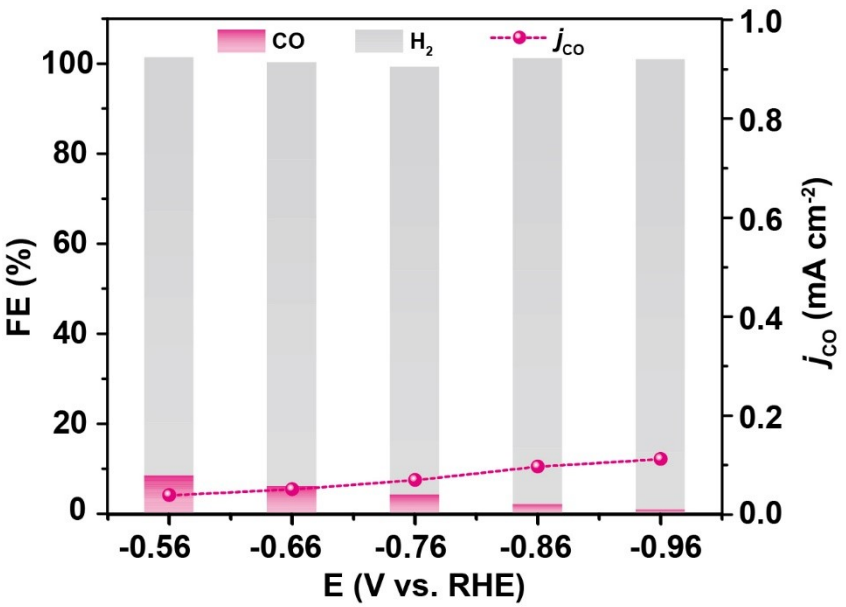

Figure S13. The ECR catalytic activity of metal-free N-doped carbon support.

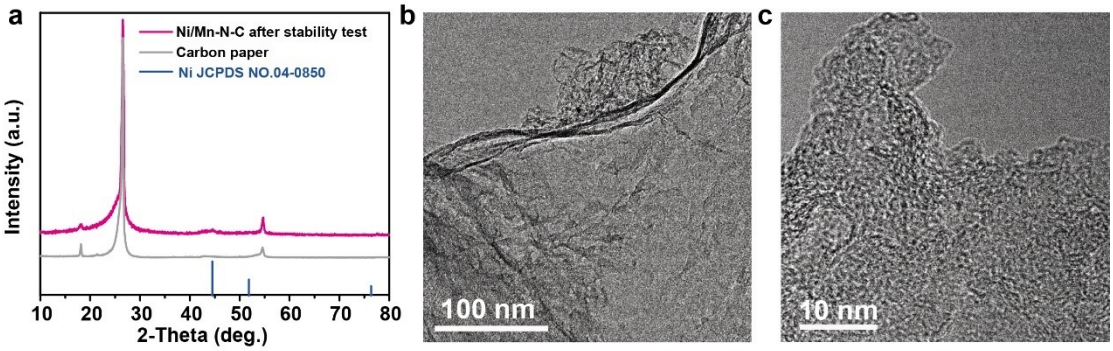

Figure S14. a) XRD pattern, b) TEM image and c) HRTEM image of Ni/Mn-N-C after CO_2RR stability test.

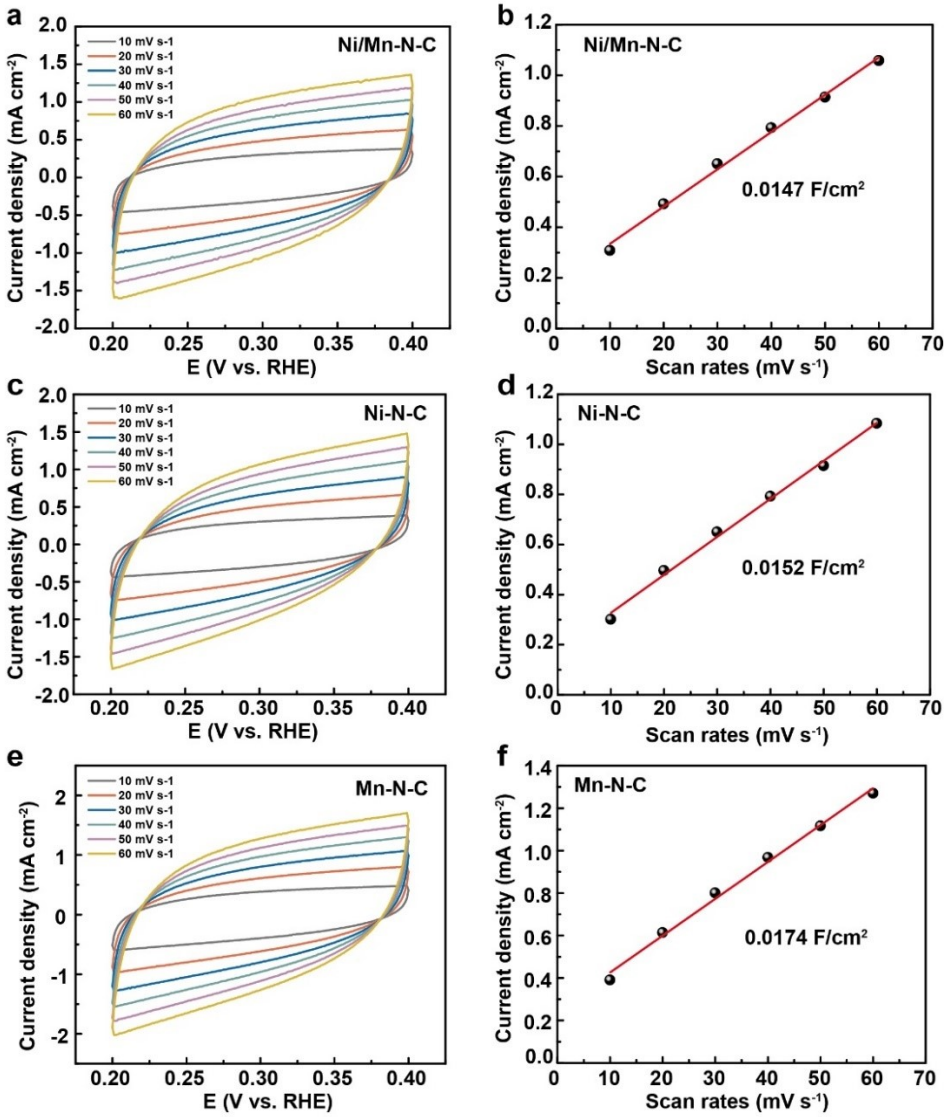

Figure S15. a) Cyclic voltammetry curves of the Ni/Mn-N-C catalyst at different scan rates, b) Double-layer capacitance (C_{dl}) of Ni/Mn-N-C catalyst. c) Cyclic voltammetry curves of the Ni-N-C catalyst at different scan rates, d) Double-layer capacitance (C_{dl}) of Ni-N-C catalyst. e) Cyclic voltammetry curves of the Mn-N-C catalyst at different scan rates, (f) Double-layer capacitance (C_{dl}) of Mn-N-C catalyst.

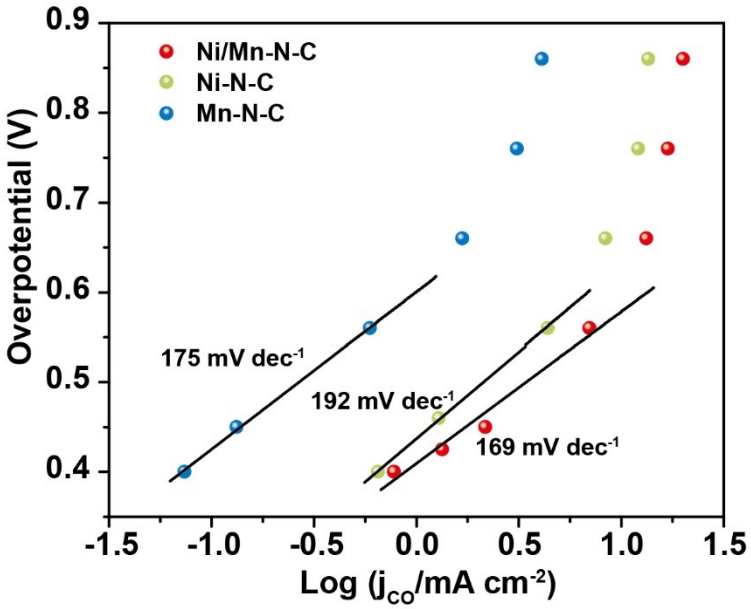

Figure S16. Tafel plots of the as-prepared samples.

Supporting Table

Table S1. Elemental contents calculated from ICP-AES results.

Sample	Ni/ICP-AES (wt%)	Mn/ICP-AES (wt%)
Ni/Mn-N-C	3.14	2.68
Ni-N-C	6.83	-
Mn-N-C	-	5.50

Table S2. Comparison of other Ni SACs for the electrochemical conversion of CO_2 to CO.

Catalyst	Potential (V vs. RHE)	FE_{CO} (%)	j_{CO} (mA cm^{-2})	Electrolyte
Ni/Mn-N-C	-0.76	96.6	13.3	0.5 M $KHCO_3$
Ni-NG[1]	-0.62	95	11	0.5 M $KHCO_3$
Ni-N_x-C[2]	-0.7	85	9.5	0.1 M $KHCO_3$
NiN-GS[3]	-0.82	93.2	4	0.1 M $KHCO_3$
Ni-N_4/C-NH_2[4]	-0.7	96	63.6	0.5 M $KHCO_3$
Ni-N_3-V[5]	-0.9	95	62.5	0.5 M $KHCO_3$
NiSA-N-CNTs[6]	-0.7	90	31.5	0.5 M $KHCO_3$
N^{2+}@NG[7]	-0.68	92	9.4	0.5 M $KHCO_3$
Ni-NG-900[8]	-1.0	94	59.6	0.5 M $KHCO_3$
NC-CNTs (Ni)[9]	-1.0	90	8.1	0.1 M $KHCO_3$

Reference:

1. K. Jiang, S. Siahrostami, T. Zheng, Y. Hu, S. Hwang, E. Stavitski, Y. Peng, J. Dynes, M. Gangisetty, D. Su, K. Attenkofer and H. Wang, *Energy Environ. Sci.*, 2018, **11**, 893-903.
2. W. Ju, A. Bagger, G.-P. Hao, A. S. Varela, I. Sinev, V. Bon, B. Roldan Cuenya, S. Kaskel, J. Rossmeisl and P. Strasser, *Nat. Commun.*, 2017, **8**, 944.
3. K. Jiang, S. Siahrostami, A. J. Akey, Y. Li, Z. Lu, J. Lattimer, Y. Hu, C. Stokes, M. Gangishetty, G. Chen, Y. Zhou, W. Hill, W.-B. Cai, D. Bell, K. Chan, J. K. Nørskov, Y. Cui and H. Wang, *Chem*, 2017, **3**, 950-960.
4. Z. Chen, X. Zhang, W. Liu, M. Jiao, K. Mou, X. Zhang and L. Liu, *Energy Environ. Sci.*, 2021, **14**, 2349-2356.
5. X. Rong, H.-J. Wang, X.-L. Lu, R. Si and T.-B. Lu, *Angew. Chem. Int. Ed.*, 2020, **59**, 1961-1965.
6. Y. Cheng, S. Zhao, B. Johannessen, J.-P. Veder, M. Saunders, M. R. Rowles, M. Cheng, C. Liu, M. F. Chisholm, R. De Marco, H.-M. Cheng, S.-Z. Yang and S. P. Jiang, *Adv. Mater.*, 2018, **30**, 1706287.
7. W. Bi, X. Li, R. You, M. Chen, R. Yuan, W. Huang, X. Wu, W. Chu, C. Wu and Y. Xie, *Adv. Mater.*, 2018, **30**, 1706617.
8. R. Boppella, M. Austeria P, Y. Kim, E. Kim, I. Song, Y. Eom, D. P. Kumar, M. Balamurugan, E. Sim, D. H. Kim and T. K. Kim, *Adv. Funct. Mater.*, 2022, **32**, 2202351.
9. Q. Fan, P. Hou, C. Choi, T.-S. Wu, S. Hong, F. Li, Y.-L. Soo, P. Kang, Y. Jung and Z. Sun, *Adv. Energy Mater.*, 2020, **10**, 1903068.